Thin-film sensing with planar terahertz metamaterials: sensitivity and limitations

John F. O'Hara[1,*]**, Ranjan Singh**[2]**, Igal Brener**[3]**, Evgenya Smirnova**[4]**, Jiaguang Han**[2]**, Antoinette J. Taylor**[1]**, and Weili Zhang**[2]

[1]*MPA-CINT, Los Alamos National Laboratory, P.O. Box 1663, MS K771, Los Alamos, New Mexico 87545*

[2]*School of Electrical and Computer Engineering, Oklahoma State University, Stillwater, Oklahoma 74078*

[3]*Sandia National Laboratories, P.O. Box 1585, MS 1082, Albuquerque, New Mexico 87122*

[4]*ISR-6, Los Alamos National Laboratory, P.O. Box 1663, MS H851, Los Alamos, New Mexico 87545*

[*]*Corresponding author: johara@lanl.gov*

Abstract: The limiting effects of varying the thickness of a dielectric overlayer on planar double split-ring resonator (SRR) arrays are studied by terahertz time-domain spectroscopy. Uniform dielectric overlayers from 100 nm to 16 μm thick are deposited onto fixed SRR arrays in order to shift the resonance frequency of the electric response. We discuss the bounds of resonance shifting and emphasize the resulting limitations for SRR-based sensing. These results are presented in the context of typical biosensing situations and are compared to previous work and other existing sensing platforms.

© 2008 Optical Society of America

OCIS codes: (160.3918) Metamaterials; (300.6495) Spectroscopy, terahertz; (170.0170) Medical optics and biotechnology

References and links

1. P. H. Siegel, "Terahertz technology in biology and medicine," IEEE Trans. Microwave Theory Tech. **52**, 2438 (2004).
2. E. R. Brown, J. E. Bjarnason, T. L. J. Chan, A. W. M. Lee, and M. A. Cells, "Optical attenuation signatures of *Bacillus subtillis* in the THz region," Appl. Phys. Lett. **84**, 3438–3440 (2004).
3. D. L. Woolard, E. R. Brown, M. Pepper, and M. Kemp, "Terahertz frequency sensing and imaging: A time of reckoning future applications?," Proc. IEEE **93** 1722–1743 (2005).
4. J. Barber, D. E. Hooks, D. J. Funk, R. D. Averitt, A. J. Taylor, and D. Babikov, "Temperature-dependent far-infrared spectra of single crystals of high explosives using terahertz time-domain spectroscopy," J. Phys. Chem. A **109**, 3501 (2005).
5. J. Chen, Y. Chen, H. Zhao, G. J. Bastiaans, and X.-C. Zhang, "Absorption coefficients of selected explosives and related compounds in the range of 0.1-2.8 THz," Opt. Express **19**, 12060 (2007).
6. B. M. Fischer, M. Walther, and P. Uhd Jepsen, "Far-infrared vibrational modes of DNA components studied by terahertz time-domain spectroscopy," Phys. Med. Biol. **47**, 3807–3814 (2002).
7. J. Zhang, and D. Grischkowsky, "Waveguide terahertz time-domain spectroscopy of nanometer water layers," Opt. Lett. **29**, 1617 (2004).
8. M. Nagel, P. Haring-Bolívar, M. Brucherseifer, H. Kurz, A. Bosserhoff, and R. Büttner, "Integrated planar terahertz resonators for femtomolar sensitivity label-free detection of DNA hybridization," Appl. Opt. **41**, 2074 (2002).
9. M. Nagel, F. Richter, P. Haring-Bolívar, and H. Kurz, "A functionalized THz sensor for marker-free DNA analysis," Phys. Med. Biol. **48**, 3625 (2003).
10. C. K. Tiang, J. Cunningham, C. Wood, I. C. Hunter, and A. G. Davies, "Electromagnetic simulation of terahertz frequency range filters for genetic sensing," J. Appl. Phys. **100**, 066105-1–3 (2006).

11. T. Baras, T. Kleine-Ostmann, and M. Koch, "On-chip THz detection of biomaterials: a numerical study," J. Biol. Phys. **29**, 187 (2003).
12. M. Brucherseifer, M. Nagel, P. Haring-Bolívar, H. Kurz, A. Bosserhoff, and R. Büttner, "Label-free probing of the binding state of DNA by time-domain terahertz sensing," Appl. Phys. Lett. **77**, 4049 (2000).
13. T. Driscoll, G. O. Andreev, D. N. Basov, S. Palit, S. Y. Cho, N. M. Jokerst, and D. R. Smith, "Tuned permeability in terahertz split-ring resonators for devices and sensors," Appl. Phys. Lett. **91**, 062511 (2007).
14. C. Debus and P. Haring Bolivar, "Frequency selective surfaces for high sensitivity terahertz sensing," Appl. Phys. Lett. **91**, 184102 (2007).
15. M. Kafesaki, Th. Koschny, R. S. Penciu, T. F. Gundogdu, E. N. Economou, and C. M. Soukoulis, "Left-handed metamaterials: detailed numerical studies of the transmission properties," J. Opt. A: Pure Appl. Opt. **7**, S12 (2005).
16. A. K. Azad, J. Dai, and W. Zhang, "Transmission properties of terahertz pulses through subwavelength double split-ring resonators," Opt. Lett. **31**, 634 (2006).
17. D. Grischkowsky, S. Keiding, M. van Exter, and Ch. Fattinger, "Far-infrared time-domain spectroscopy with terahertz beams of dielectrics and semiconductors," J. Opt. Soc. Am. B **7**, 2006 (1990).
18. W. J. Padilla, A. J. Taylor, C. Highstrete, Mark Lee, and R. D. Averitt, "Dynamical electric and magnetic meta-material response at terahertz frequencies," Phys. Rev. Lett. **96**, 107401 (2006).
19. J. B. Pendry, A. J. Holden, D. J. Robbins, and W. J. Stewart, "Magnetism from conductors and enhanced nonlinear phenomena," IEEE Trans. Microwave Theory Tech. **47**, 2075 (1999).
20. J. D. Baena, J. Bonache, F. Martín, R. Marqués Sillero, F. Falcone, T. Lopetegi, M. A. G. Laso, J. García-García, I. Gil, M. F. Portillo, and M. Sorolla, "Equivalent-circuit models for split-ring resonators and complementary split-ring resonators coupled to planar transmission lines," IEEE Trans. Microwave Theory Tech. **53**, 1451 (2005).
21. J. F. O'Hara, E. Smirnova, A. K. Azad, H.-T. Chen, and A. J. Taylor, "Effects of microstructure variations on macroscopic terahertz metafilm properties," Active and Passive Electronic Components **2007**, 49691 (2007).
22. J. A. Defeijter, J. Benjamins, F. A. Veer, "Ellipsometry as a tool to study adsorption behavior of synthetic and biopolymers at air-water-interface," Biopolymers **17**, 1759–1772 (1978).
23. A. Markelz, S. Whitmire, and J. Hillebrecht, et. al., "THz time domain spectroscopy of biomolecular conformational modes," Phys. Med. Biol. **47**, 3797–3805 (2002).
24. B. M. Fischer, M. Hoffmann, H. Helm, et. al., "Terahertz time-domain spectroscopy and imaging of artificial RNA," Opt. Express **13**, 5205–5215 (2005).
25. A. K. Azad, A. J. Taylor, E. Smirnova, and J. F. O'Hara, "Characterization and analysis of terahertz metamaterials based on rectangular split-ring resonators," Appl. Phys. Lett. **92**, 011119 (2008).
26. H.-T. Chen, W. J. Padilla, J. M. O. Zide, S. R. Bank, A. C. Gossard, A. J. Taylor, and R. D. Averitt, "Ultrafast optical switching of terahertz metamaterials fabricated on ErAs/GaAs nanoisland superlattices," Opt. Lett. **32**, 1620–1622 (2007).
27. M. A. Cooper, Drug Discovery Today **11**, 1061 (2006).
28. SRU Biosystems, Inc., www.srubiosystems.com.
29. Biacore Life Sciences, www.biacore.com.
30. G. U. Lee, L. A. Chrisey, E. E. O'Ferrall, D. E. Pilloff, N. H. Turner, R. J. Colton, Israel J. Chem. **36**, 81–87 (1996).

1. Introduction

The continued quest for new chemical and biological sensing modalities that avoid labeling, improve sensitivity, and take advantage of new chemical signatures has fueled a recent interest in terahertz (THz), or far-infrared, sensing [1–3]. This is mainly due to the unique properties many materials exhibit in the THz regime. Of particular interest are those materials that respond resonantly at THz frequencies, making them more amenable to sensing in small quantities. Some examples include explosives [4, 5] and DNA [6]. Detection techniques for sensing very small quantities at THz frequencies have also matured, in parallel with increasing knowledge of THz materials properties. For example, waveguide sensors have proven useful for sensing thin films of water [7] by increasing the effective interaction length. In other examples [8–11] THz micro-resonators and filters were studied to sense analytes by the frequency shift they induce on the device's resonant response. This method is reported to have increased sensitivity to the binding state of DNA samples by $\sim 10^3$ times over conventional free-space time-domain spectroscopy [8, 12].

Metamaterials and frequency selective surfaces have also arisen as candidates for highly sen-

sitive chemical or biological detection since they can be small (unit cell dimensions are typically $\lambda/10 - \lambda/5$) and show a resonant frequency response that is tunable by design. It has already been shown that small quantities of silicon (< 1 ng), deposited as a film or overlayer on a planar THz metamaterial, can shift the resonance frequency by an easily measurable amount [13]. Similarly, simulations of assymetric split-ring resonators (SRRs) indicate a possible scenario in which films as thin as 10 nm may be measured [14]. These ideas capitalize on the structure of split-ring resonators, whose natural oscillation frequencies depend critically on the permittivity of the boarding dielectrics [15]. Our work has shown good consistency with this principle: the resonance frequency of SRRs shifted from 0.80 THz to 0.51 THz by changing the substrate from fused silica to silicon [16]. In terms of practical sensing, however, the limits of this technique are clearly important as they will ultimately define the utility of the sensing approach. Here we investigate the behavior of dielectric overlayers on metamaterials, with particular relevance to sensing limitations. We first present measured THz transmission data illustrating the resonance shifting effects and then compare this to previous similar approaches. Finally, we discuss the implications in terms of practical sensing considerations.

2. Experimental

The metamaterials are fabricated by conventional photolithography techniques and consist of square arrays of double SRRs, made from optically thick 200 nm aluminum, on 0.64 mm thick silicon substrates (p-type resistivity 20 Ω-cm). The inset of Fig. 1 shows the diagram of a unit cell with dimensions $d = 5$ μm, $w = 5$ μm, $t = 5$ μm, $l = 40$ μm, and a lattice parameter of $P = 60$ μm. The dielectric overlayers are either spin coated by single-wafer spin processing (Laurell WS-400A) or deposited by thermal evaporation (BOC Edwards AUTO 306). The metamaterials are characterized in transmission by terahertz time-domain spectroscopy (THz-TDS) in a broadband, photoconductive switch based system that consists of four parabolic mirrors in a 8-F confocal geometry [16,17]. This coherent technique records both the amplitude and phase of the electric field so that complex material parameters can be obtained. The metamaterial is penetrated by the focused THz beam at normal incidence and with the polarization shown in Fig. 1. Each SRR array has a 20 mm $\times$ 20 mm clear aperture to prevent THz beam clipping. Since the incident wave's magnetic field is parallel to the plane of the SRRs, this configuration actually excites an electric response in the SRRs, which is known to occur at the same frequency as the magnetic resonance [18].

Measured resonances were observed to shift lower in frequency as the thickness of the overlayer increased. Figure 1 shows the frequency-dependent amplitude transmission of the metamaterial with and without a 16 μm thick photoresist (Futurrex, Inc.) overlayer. For all of our measurements, the metamaterial transmission was defined as the ratio of the Fourier-transformed amplitude spectra of the metamaterial sample and a reference, the reference being an unmetallized substrate identical to the SRR substrate and coated with the same overlayer. Three distinct resonances are observed as transmission dips in the uncoated metamaterial. They are the LC resonance at $\omega_{LC}/2\pi = 0.460$ THz, the electric dipole resonance at $\omega_d/2\pi = 1.356$ THz, and a weaker resonance at $\omega_i/2\pi = 1.160$ THz due to excitation of the smaller, inner SRR. As shown by the dotted curve in Fig. 1, the presence of the 16 μm thick overlayer (having a relative permittivity $\varepsilon_r = 2.7 \pm 0.2$ at 1.0 THz) causes the LC, dipole, and inner SRR resonances all to shift to lower frequencies by 36 and 60 and 78 GHz, respectively. Additional measurements characterized the metamaterial resonance frequencies as a function of overlayer thickness. These are shown for the LC and dipole resonances as open circles in Figs. 2(a) and 2(b). Though overlayers were applied up to 90 μm in thickness, the shifting effect saturated at approximately 16 μm, and no further significant shifts were observed. Finite-element simulations were also performed to verify these results. They are shown as filled circles
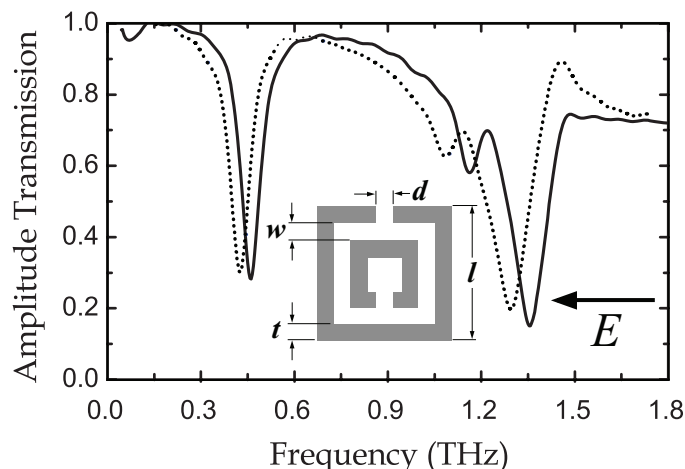
Fig. 1. Frequency-dependent amplitude transmission of a double SRR metamaterial without (solid curves) and with (dotted curves) a 16 μm thick photoresist overlayer.

in Fig. 2 and agree well with the measured data. Simulations also helped elucidate the origin of other spectral features, such as the peak at 1.5 THz in the 16 μm overlayer data shown in Fig. 1. This frequency corresponds to the onset of a higher-order mode in the Si substrate associated with the periodicity of the structure. The $\sim$1.5 THz peak becomes pronounced mainly because the overlayer induces a larger separation between this higher-order mode and the dipole mode of the SRR.

We performed additional measurements in which only 100 nm or 200 nm of B_2O_3 ($\varepsilon_r = 3.6 \pm 0.2$ at 1.0 THz) was thermally evaporated on a slightly different, but similar, metamaterial sample. In this case a 270 nm SiO_2 layer was deposited on the Si surface before metallization and served to prevent diffusion of B_2O_3 into the Si substrate. Even with the 100 nm layer, a measurable shift is observed in the resonances indicating the sensitive manner in which these samples respond to their dielectric environment. The LC and dipole resonances are shown in Figs. 3(a) and 3(b), respectively. The frequency shifts are 2-3 GHz for the 100 nm overlayer, and 4-5 GHz for the 200 nm film. A 2 GHz shift for a resonance at 1.426 THz represents a shift of only one part in 713 or 0.14%. For the resonance at 0.503 THz this is a 0.40% shift. These steps are about 10-30 times smaller than previously reported results [13], and given the low resonator Q factors, effectively represent a continuous adjustability in the resonance frequency.

3. Discussion

3.1. Analysis of experimental results

We now discuss the implications of the measured data with respect to sensing limitations inherent in these metamaterials. While a 2-3 GHz resonance shift is both measurable and repeatable in our data, it is certainly approaching the *minimum* measurable change for this experimental configuration. Systems in which noise or sensor contamination is a larger issue would obviously require greater resonance shifts for positive identification. Since the measured resonance shifts were due to alterations in the SRR capacitance, one can formulate a quantitative approach to determining the limitations of SRRs as sensors. It begins by utilizing the RLC circuit model of the SRR, a valid and commonly used approach for describing SRR behavior [19–21]. In this case the resonance frequency is defined as $\omega_0 = (LC)^{-1/2}$, where C and L are the capacitance and inductance of the SRR, respectively. As such, the change in resonance frequency as a function
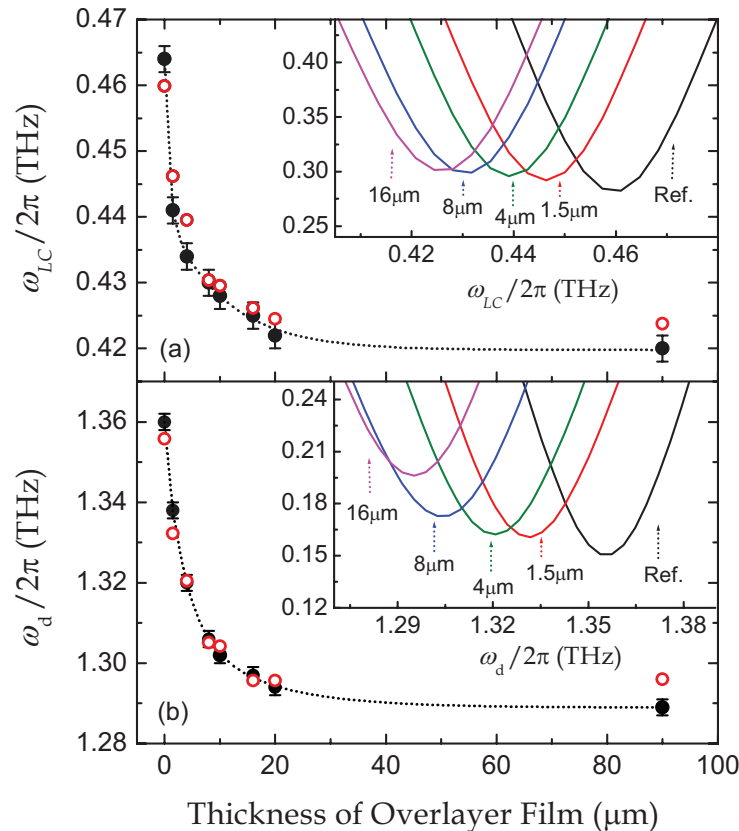
Fig. 2. (a) LC (ω_{LC}) and (b) electric dipole (ω_d) resonance frequencies as a function of overlayer thickness. Measured and simulated results are represented by open and closed circles respectively, with dotted curves as a guide to the eye. The insets show the measured amplitude transmission around the LC and dipole resonances for various overlayer thicknesses.

of capacitance can be derived as $d\omega_0 = -L/2(LC)^{-3/2}dC$. Expressed in terms of percentage change, $d\omega_0/\omega_0 = -dC/(2C)$. Since ω_0 is a non-linear function of C these derivatives are only useful for linking *small* changes in dC and $d\omega_0$; this is generally satisfied in our case. Using the equations, a 2 GHz resonance redshift corresponding to $d\omega_0/\omega_0 = -0.4\%$ (at 0.503 THz) is caused by a 0.8% increase in SRR capacitance. It is generally accepted that most of the capacitive response of a SRR occurs in a small volume surrounding the ring gaps [13, 14]. This is due to the strong field enhancement commonly observed there. However, our measured data shows that this enhancement is not quite as useful for sensing as it first appears. The 100 nm B_2O_3 overlayer half fills all the regions (ring gaps and space between rings) bound by the 200 nm thick aluminum. Even with strong electric field concentration, this significant gap alteration only results in a ~0.8% change in the net SRR capacitance.

The limitations to this sensing modality become apparent. A metamaterial array based on a high-permittivity substrate will have a large, and likely majority, capacitive contribution *in the substrate*. Obviously, the sensed layer cannot penetrate the substrate or interact with any of the electric flux contained therein. This substantially dilutes the change in capacitance and decreases the amount of resonance shift due to the overlayer. Though thinner substrates would
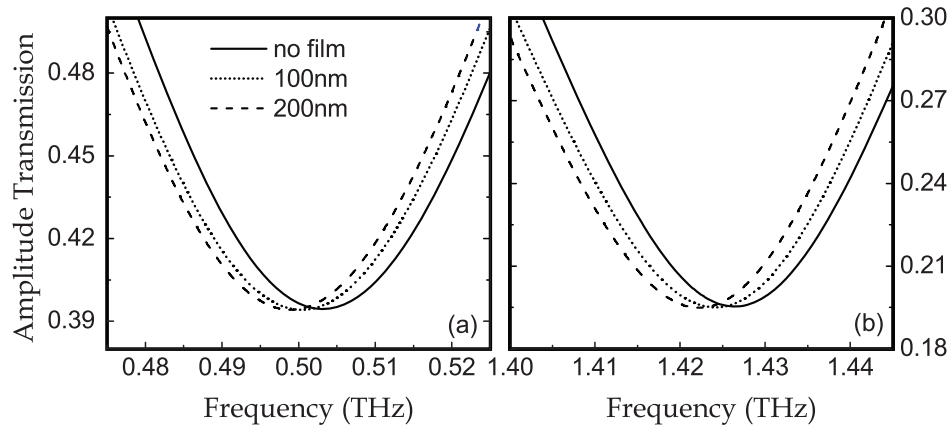
Fig. 3. Measured amplitude transmission at (a) LC and (b) dipole resonances of a double SRR metamaterial with a B_2O_3 nano-overlayer film.

certainly improve the situation, it's clear from the saturated resonance shift data of Fig. 2 that a substrate of only 10-20 μm is sufficient to maximize this dilution effect. Such thin substrates obviously cause great fabrication and durability challenges. This is only one manifestation of the overarching limit to sensing with metamaterials: there is critical volume of electric flux which must be contained within the sensed layer to cause a measurable resonance shift. Yet another instance is revealed by the saturated resonance data. From Fig. 2 we can surmise that SRR fringing fields extend out to roughly 16 μm. Again, this represents electric flux that is *not* contained directly within the SRR gaps. As such, any sensed layer confined to the gaps would have no interaction with this fringing flux, thus reducing its effect on the measured resonance. These considerations indicate that THz sensing of low-volume layers (i.e. single-molecule layers, functionalized receptor planes, low-density airborne species, etc.) using metamaterials on thick, high-index substrates faces a number of possible challenges, in spite of potentially large sample permittivities.

3.2. *Static dielectric effects*

Given the limitations defined by the data we can estimate how much the situation could be improved by altering the metamaterial substrate. What follows is an extrapolation of the measured results that permits an estimation of the sensing limitations of our ring design. The same procedure could be applied to measurements of any similar metamaterial, however the specific numbers involved would change. The minimum sample volume which *could* be sensed with a substrate-free metametamaterial design (or free-standing metamaterial) can be approximated by first assuming that the electric flux distribution on either side of the plane of our Si-based SRR is spatially symmetric. The symmetry here refers only to the shape of the flux distribution, not its density, which is greater in the substrate due to its high permittivity. This implies that the substrate-bound flux accounts for roughly 90% of the total SRR capacitance. The total SRR capacitance is then modeled as four parallel capacitors: C_1 being the capacitance due to flux within the substrate, C_{2a} due to flux within the air filled fraction of the gap volumes, C_{2d} due to flux within the overlayer filled fraction of the gaps, and C_3 due to fringing flux in air. If the 0.8% measured capacitance shift is due only to dielectric changes in the gap volumes, then it can be shown that $C_{2a} + C_{2d}$ only accounts for about 0.6% of the total SRR capacitance, C_0.

The derivation is as follows. The total capacitance is given by

$$C_0 = C_1 + C_{2a} + C_{2d} + C_3$$
$$= C_1 + A f_a \varepsilon_0 + A(1 - f_a)\varepsilon_d + C_3$$

where A is a scaling constant, f_a is the fraction of the gaps filled by air, and ε_0 and ε_d are the permittivities of free-space and of the overlayer, respectively. For fully air filled gaps, $C_0 = C_1 + A\varepsilon_0 + C_3$. For half filled gaps, as is the case in the 100 nm B_2O_3 overlayer, $1.008C_0 = C_1 + A\varepsilon_0/2 + A\varepsilon_d/2 + C_3$. Assuming C_1 and C_3 do not change by the addition of the overlayer, then the difference of these equations is $0.008C_0 = A(\varepsilon_0/2 + \varepsilon_d/2 - \varepsilon_0)$, which for $\varepsilon_d = 3.6\varepsilon_0$ equals $1.3A\varepsilon_0$, or $A\varepsilon_0 = 0.006C_0 = C_{2a} + C_{2d}$. Similar calculations can be used to obtain a general capacitive loading equation describing the effect of changing the substrate, or the permittivity or thickness of the overlayer. We stress that the following expression is only approximate, being based on an extrapolation of our measured data. It is applicable only to our metamaterial design and under the assumption of a thick substrate ($> 20\ \mu$m) and thin overlayers (≤ 200 nm).

$$\frac{d\omega_0}{\omega_0} = -\frac{0.006154(\varepsilon_d/\varepsilon_0 - 1)(1 - f_a)}{2 - 0.18966(9.48 - \varepsilon_s/\varepsilon_0)}$$

where ε_s is the substrate permittivity and the remaining variables retain their previous definitions. The equation shows that after replacing the substrate with air ($\varepsilon_s = \varepsilon_0$), the volume fraction of the gaps filled by B_2O_3 must be about 10% (20 nm thick) to cause a 0.4% shift in the LC resonance. This is a substantial improvement over the 50% gap filling necessary for the silicon based metamaterial. Some care must be exercised in calculations involving a substrate permittivity different than the measured one. In such cases, ω_0 also changes, so we prefer to leave resonance shifts in terms of percentage rather than absolute values.

3.3. Comparisons with simulations and previous work

Our results can now be compared to simulations and to results obtained by other studies. As shown in Fig. 2, the agreement between measured and simulated resonance shifts is quite adequate for the cases in which the overlayer was $\geq 1.5\ \mu$m thick. Additional simulations were performed for the B_2O_3 overlayers. These simulations were qualitatively very similar to the data, though redshifted about 35 GHz in frequency. They also showed a slightly greater resonance shift than the measurements, causing, for example, a 5 GHz shift for the 100 nm layer as opposed to the measured 2 GHz. Further simulations produced other disagreements and even counterintuitive results that are currently under investigation. For example, simulated resonance shifts were even greater when the B_2O_3 overlayer was selectively removed from the top of the metal. This would be expected to decrease the net capacitance change and thereby cause a smaller, not greater, resonance shift. Non-uniformities or voids in the actual overlayers are one possible problem, though the layers appear quite uniform under microscopic inspection. Another possible problem is accounting for all of the experimental variables in the simulation. In our investigations, fabrication imperfections seem to be amplified in simulations involving thin films, which are already troublesome. For this reason, we cautiously emphasize the importance of careful experimental verification, especially in cases of very thin overlayers.

The resonance shifts we observe are quite small compared to those measured in Driscoll, *et. al.* [13]. In their case, the shift observed after adding a single overlayer to the metamaterial was about 30 GHz. A strict comparison to our measurements is difficult because their method of overlayer application was very different. Despite this, the results are fairly consistent with ours. They used an overlayer of Si nanospheres (50 nm diameter) which have a much higher permittivity than B_2O_3. Using the capacitive loading equation, we estimate that a 151 nm overlayer of Si ($f_a = 0.24$, $\varepsilon_d = 11.7\varepsilon_0$) on our structure ($\varepsilon_s = 9.48\varepsilon_0$) would shift the resonance about

2.5%. For a resonance centered at 1.20 THz, as in Driscoll *et. al.*, this would cause a 30 GHz shift.

Strict comparison to the work of Debus, *et. al.* [14] is also difficult for several reasons. In their work, a ring of substantially different design was simulated on an unspecified substrate and with an analyte of unspecified permittivity. Furthermore, their array was probed with wave polarization effectively parallel to the gaps, instead of across the gaps. Due to symmetry, our design would not even exhibit the LC resonance with such a polarization [16]. In terms of sensing, the main advantage of their ring design is the steep resonance flank that changes the reflection by about 7 dB per 4 GHz of shift. Their design appears to utilize two, closely spaced, ring resonances that couple to (interfere with) one another to create a single sharp response. This further illustrates how alternative metamaterial or frequency selective surface designs can be utilized to enhance sensing. Coupled resonance techniques are further discussed in the following section. Comparatively, our design is not optimized for thin-film sensing, but utilizes a single Lorentzian resonance that shows a maximum change of 2 dB per 11 GHz of shift. Our metamaterial configuration emphasizes adherence to the effective medium approximation. As such, the ring dimensions are 15 times smaller than the resonant wavelength; this ratio is 3.5 in the Debus *et. al.* work. This affects sensing mainly in terms of volumes of analyte. In the Debus *et. al.* work, a sensed volume of 10 nm $\times$ 27.5 μm $\times$ 27.5 μm $= 7.56\ \mu$m^3 was sufficient to induce a measurable shift in the resonance around 0.9 THz. In our work, the B_2O_3 was deposited in all the ring regions, including the ring gaps and also the spaces between the two rings. This resulted in a measurable shift at 0.5 THz. If we assume that most of this effect was due to analyte deposited within the ring gaps, then the pertinent volume of sensed material is about 2×100 nm $\times$ 5 μm $\times$ 5 μm $= 5\ \mu$m^3. A measurable shift derived by filling the ring gaps alone would likely require somewhat more material. Nevertheless, the actual sensed volume in both designs appears quite comparable, even if it takes the form of a thinner layer in the Debus *et. al.* work.

3.4. *Resonant dielectric and absorption effects*

We now point out some possibly significant sensing advantages available by utilizing analyte resonances. The idea is to fabricate a sensor whose resonance is tuned to overlap a resonant line of the analyte. Over certain frequency ranges, changes in the analyte composition can cause large changes in permittivity. Variables including rotational-vibrational degrees of freedom, binding state, degrees of hydration, conformation, etc., can all cause large permittivity shifts. This is particularly true in the THz regime, as opposed to visible wavelengths [22]. For example, THz relative permittivities (ε_r) range from 2.9–3.2 in bovine serum albumin (BSA) [23], 2.0–2.5 in DNA [6] and 2.5–4 in RNA [24]. As an example at THz frequencies, short strands of DNA go from $\varepsilon_r = 2.0$ to 2.3 upon hybridization. Using our data, we can provide a useful estimate, in a biosensor context, of the resonance sensitivity to such changes in the overlayer permittivity. Using the capacitive loading equation, a change of conformation in a uniform 50 nm DNA layer located in the SRR gaps would result in a 0.1% resonance shift if the metamaterial was free-standing. The same layer would shift the resonance by 0.02% or 0.1 GHz in our SiO_2/Si backed metamaterial. To achieve a measurable 0.4% resonance shift in the free-standing metamaterial of our ring design we estimate the hybridizing DNA layer would have to be 170 nm thick, filling approximately 85% of the SRR gaps. This thickness is well above the single monolayer value used in typical DNA microarrays.

There is another scenario that must be considered with resonant analytes. This is the case in which the SRR resonance is re-shaped due to coupling or interference with the analyte's resonance. Coupled resonators can drastically change the overall response of a system as is well-evidenced by myriad physical systems, THz metamaterials included [21, 25]. Atomic line-

splitting induced by magnetic fields (Zeeman splitting) is a good example. For this to be a significant effect in our metamaterials two conditions must be satisfied: 1) the oscillator strengths of both resonators (the SRR and the analyte) must be of sufficient strength, and 2) the coupling between the resonances must be sufficiently strong. The latter condition is likely the limiting factor for metamaterial sensing. Again, the main obstacle is the small amount of electric flux linking the SRR and the analyte. Flux that is not contained in the sample cannot serve as a resonance coupling agent. Monolayers are typically < 10 nm thick, therefore we would expect very little linkage to our SRR resonance and a very small resonance change. Also, given the size of the gap, the monolayer would contain a relatively small number of macromolecules, resulting in a low oscillator strength. For these reasons, we don't expect resonance coupling to have a strong reshaping effect, though a subtle effect might be enough for positive identification in a well-tuned or optimized system.

We also address the possibility of using the analyte absorption as a sensing modality. Previous THz metamaterial work [18, 26] has shown that large resonance damping effects can be caused by relatively small Ohmic losses in the SRR gap. In that work, currents induced in the SRR by the incident THz field were quickly damped by absorption within the photodoped semiconductor substrate. The same principle may be applicable to sensing. In this case an absorptive analyte placed in the SRR gap would damp the overall resonance, creating a measurable change. However, with low macromolecule quantities and approximate molar absorption coefficients of < 100 (M·cm)$^{-1}$ at THz frequencies, such small samples would likely produce very little damping.

3.5. Comparison with other biosensor platforms

Finally, it is useful to compare the sensitivity, advantages, and disadvantages of the device analyzed in this paper to more established label-free biosensor platforms, an issue commonly overlooked in THz oriented work. Most of the label-free biosensor platforms measure mass-loading over a finite sensing area, and thus sensitivities are quoted in units of pg/mm^2. Examples of non-optical techniques include quartz microbalances and surface acoustic wave sensors, with reported sensitivities in the range of 5–200 pg/mm^2. A number of commercial optical biosensors have mass sensing resolutions ranging from 0.1–5 pg/mm^2 [27] over areas ranging from 50 μm^2 [28] to 23,000 μm^2 [29]. These mass resolution ranges allow detection of relatively small compounds ($\sim$ 100's of daltons (Da)) on larger immobilized targets (10's of kDa). In DNA hybridization, one typically measures the addition of 7–10 kDa oligo fragments to immobilized short strands, but with very small changes in overall thickness [30]. We can compare our device to these systems by knowing that the aforementioned mass-loading translates into a thickness resolution on the order of a few nanometers to achieve monolayer sensitivity to macromolecules. For example, a monolayer of BSA adsorbs with a thickness of 4.5 nm [22]. Adsorbed thickness is only 2 nm for 20-base long double-stranded DNA [30]. The results of our experimental analysis show such fine thickness resolution is obviously unattainable with our devices. On the other hand, the THz regime offers large changes in permittivity associated with these macromolecule layers, a feature unavailable to optical sensors. Therefore, with improved metamaterial designs, these goals could be within reach in the near future.

4. Summary

In conclusion, we have performed THz-TDS measurements on planar metamaterials with various dielectric overlayers. These data can be used to investigate the limitations and obstacles of using THz metamaterials as sensing devices. We have found that for our particular metamaterial design an overlayer of 100 nm is quickly approaching the limit of detectability. Our results are largely consistent with previous findings. However, measured results were

not always in good agreement with simulations, particularly those involving very thin films (<200 nm). This strongly points to the necessity of experimental verification, not only to properly structure future simulations, but also to reveal the practical difficulties of analyte deposition on split-ring based sensors. Finally, our results illustrate many of the factors involved in sensing optimization, such as ring geometry, substrate composition, analyte composition and deposition, resonance effects, and limitations of the THz measurement system. Previous works [13, 14] have also discussed how some of these optimization variables might be utilized in future metamaterials and frequency selective surface based sensors. Such work presents a promising outlook for THz sensing technology.